Alzheimer's Research & Therapy

RESEARCH

Open Access

Selection of the optimal channel configuration for implementing wearable EEG devices for the diagnosis of mild cognitive impairment

Kyeonggu Lee[1], Kang-Min Choi[1], Seonghun Park[1], Seung-Hwan Lee[2,3] and Chang-Hwan Im[1,4*]

Abstract

Background: Early diagnosis of mild cognitive impairment (MCI) is essential for timely treatment planning. With recent advances in the wearable technology, interest has increasingly shifted toward computer-aided self-diagnosis of MCI using wearable electroencephalography (EEG) devices in daily life. However, no study so far has investigated the optimal electrode configurations for the efficient diagnosis of MCI while considering the design factors of wearable EEG devices. In this study, we aimed to determine the optimal channel configurations of wearable EEG devices for the computer-aided diagnosis of MCI.

Method: We employed an EEG dataset collected from 21 patients with MCI and 21 healthy control subjects. After evaluating the classification accuracies for all possible electrode configurations for the two-, four-, six-, and eight-electrode conditions using a support vector machine, the optimal electrode configurations that provide the highest diagnostic accuracy were suggested for each electrode condition.

Results: The highest classification accuracies of 74.04% ± 4.82, 82.43% ± 6.14, 86.28% ± 2.81, and 86.85% ± 4.97 were achieved for the optimal two-, four-, six-, and eight-electrode configurations, respectively, which demonstrated the possibility of precise machine-learning-based diagnosis of MCI with a limited number of EEG electrodes. Additionally, further simulations with the EEG dataset revealed that the optimal electrode configurations had significantly higher classification accuracies than commercial EEG devices with the same number of electrodes, which suggested the importance of electrode configuration optimization for wearable EEG devices based on clinical EEG datasets.

Conclusions: This study highlighted that the optimization of the electrode configuration, assuming the wearable EEG devices can potentially be utilized for daily life monitoring of MCI, is necessary to enhance the performance and portability.

Keywords: Mild cognitive impairment, Electroencephalography, Wearable EEG device, Machine learning, Optimal channel configuration

Introduction

Mild cognitive impairment (MCI) is a psychiatric syndrome characterized by a cognitive decline greater than that expected based on an individual's age and education level [1]. MCI is believed to be associated with several underlying causes, especially for Alzheimer's disease

*Correspondence: ich@hanyang.ac.kr

[1] School of Electronic Engineering, Hanyang University, Seoul, Republic of Korea
Full list of author information is available at the end of the article

(AD) [2]. As approximately 40–60% of patients with MCI have an underlying AD pathology [3, 4], early detection of MCI is important for postponing cognitive decline and preventing its conversion to AD [5]. In general, however, a patient's visit to the hospital for the diagnosis of MCI is considerably delayed because MCI does not usually interfere with daily activities, and individual symptoms are heterogeneous depending on the etiology and cognitive reserve [6, 7]. Moreover, conventional methods for diagnosing MCI such as history recording, clinical questionnaires, and simple cognitive tests are susceptible to misdiagnosis particularly in the early stages of MCI [8]. The exploration of all cognitive domains and quantification of overall cognitive performance are essential for avoiding potential diagnostic errors. However, such a time-consuming and tedious diagnostic procedure might act as a barrier preventing the early detection of MCI by discouraging potential patients from visiting a medical clinic [7].

Various biomarkers have been suggested for a more quantitative and objective diagnosis of MCI such as those extracted from cerebrospinal fluid (CSF), magnetic resonance imaging (MRI), and electroencephalography (EEG) [7, 9–11]. Recently, biomarkers from EEG have drawn increased attention owing to their advantages of relatively shorter diagnostic time and higher cost-effectiveness [12–15]. The key characteristics of the EEG data of elderly patients with MCI compared with those of normal elderly people (without MCI) are reduced complexity, decrease in inter-regional synchronizations, and shifts in the power spectrum from high-frequency components (alpha, beta, and gamma bands) toward low-frequency components (delta and theta bands) [16, 17]. These EEG biomarkers have been widely employed for the computer-aided diagnosis of MCI based on machine learning (ML) algorithms, thus demonstrating the possibility of a reliably high-performance EEG-based diagnosis of MCI [17–21]. For example, Morabito et al. [20] achieved an accuracy of 85% in classifying MCI and healthy control subjects (HCs) using a convolutional neural network (CNN) model. Fiscon et al. [21] achieved a classification accuracy of 92% for the detection of MCI using a decision tree classifier with wavelet coefficients from the EEG data.

However, previous studies on machine learning-based MCI diagnoses with EEG have generally employed research-grade EEG devices that require the aid of a trained experimenter so that the wider utilization of EEG-based MCI diagnosis in places other than laboratory or clinical environments is prevented [22–24]. Recent developments in wearable EEG technology have made EEG devices portable and inexpensive, thereby expanding their application fields [24–26]. For example, wearable EEG devices have the potential to be used for the early detection of neurological diseases [27, 28]. With the recent developments of hydrogel electrode technologies, it is expected that wearable EEG devices would be widely employed for continuous, long-term EEG monitoring and daily-life diagnosis of neurological diseases [29]. In this regard, these devices could be effective tools in the primary screening of MCI, for which early diagnosis is generally difficult due to the delayed visit to the hospital.

To increase the effectiveness of wearable EEG devices, it is necessary to increase the accessibility of the patients by making the devices portable and affordable [30]. Although attempts have been made to reduce the number of EEG channels while preserving the performance of the devices [31] and to investigate the optimal channel configurations that maximize the performance in brain-computer interfaces and biometric systems [32, 33], to the best of our knowledge, no study was performed to investigate the optimal electrode configurations for wearable EEG devices to maximize the accuracy of the machine learning-based diagnosis of MCI.

In this paper, we present a procedure to determine the optimal electrode configurations for wearable EEG devices to diagnose MCI, considering both the practicality and classification accuracy of wearable EEG devices. We suggest optimal channel configurations for two-, four-, six-, and eight-electrode conditions using a clinical EEG dataset collected from patients with MCI and healthy individuals. Furthermore, we demonstrate that the proposed optimal electrode configurations exhibit statistically higher performance in the diagnosis of MCI than commercial wearable EEG devices.

Methods and materials

Determination of optimal electrode configuration

To determine the optimal electrode configurations for different numbers of electrodes, we only considered configurations consisting of electrode pairs positioned symmetrically with respect to the midline (e.g., F7–F8 and FC5–FC6) and electrodes located on the midline (e.g., Fz and Pz), because it was thought that wearable EEG devices with bilateral symmetry are much easier to implement than configurations with randomly distributed electrodes [27]. In other words, the optimal electrode configurations were determined by comparing the classification accuracies of all possible electrode configurations that can be formed with the combinations of midline electrodes (Fz, Cz, Pz, and Oz) and symmetric electrode pairs (Fp1–Fp2, AF3–AF4, F7–F8, F3–F4, FC5–FC6, FC1–FC2, T7–T8, C3–C4, CP5–CP6, CP1–CP2, P7–P8, P3–P4, PO3–PO4, and O1–O2) when the number of electrodes was set to two, four, six, and eight.

The number of all possible electrode combinations for the two-, four-, six-, and eight-electrode configurations were 20, 176, 924, and 3276, respectively.

The optimal electrode configuration was determined by selecting the electrode configuration that exhibited the highest accuracy among all possible channel combinations. After determining the optimal electrode configurations with two, four, six, and eight electrodes, the classification accuracies of the optimal electrode configurations were compared with those of commercial wearable EEG devices including Focusband™ (T2 Green Pty Ltd.; Carrara, QLD, Australia), Insight™ (Emotiv Inc.; San Francisco, CA, USA), DSI-7™ (Wearable Sensing LLC; San Diego, CA, USA), Imec™ (Imec Inc.; Leuven, FB, Belgium), and EPOC™ (Emotiv Inc.; San Francisco, CA, USA). The electrode configurations of commercial devices are shown in Fig. 1.

Participants

EEG data were acquired from 42 participants (21 patients with MCI and 21 healthy controls [HCs]) at the Inje University Ilsan Paik Hospital. The diagnosis of MCI was based on a clinical evaluation by trained psychiatrists who used the Structured Clinical Interview for DSM-IV (or V) Axis I Disorders (SCID-I) or the Mini International Neuropsychiatric Interview (MINI). None of the patients who participated in the study were pregnant or had any of other neurological or comorbid disorders, organic brain damage, or impairments in sensory or motor functions.

A total of 21 healthy participants were recruited from the local community. They did not satisfy the DSM-IV or V-based lifetime diagnostic criteria for any major psychiatric disorder as screened by the SCID-I Non-Patient Edition (SCID-NP) or MINI-based diagnostic criteria.

Demographic information, including sex, age, and education, was compared between the patients with MCI and HCs. A measurement of educational level is based on the duration of formal education. There were no statistically significant differences between the two groups in terms of demographic characteristics, including sex, age, and education. The detailed demographic information

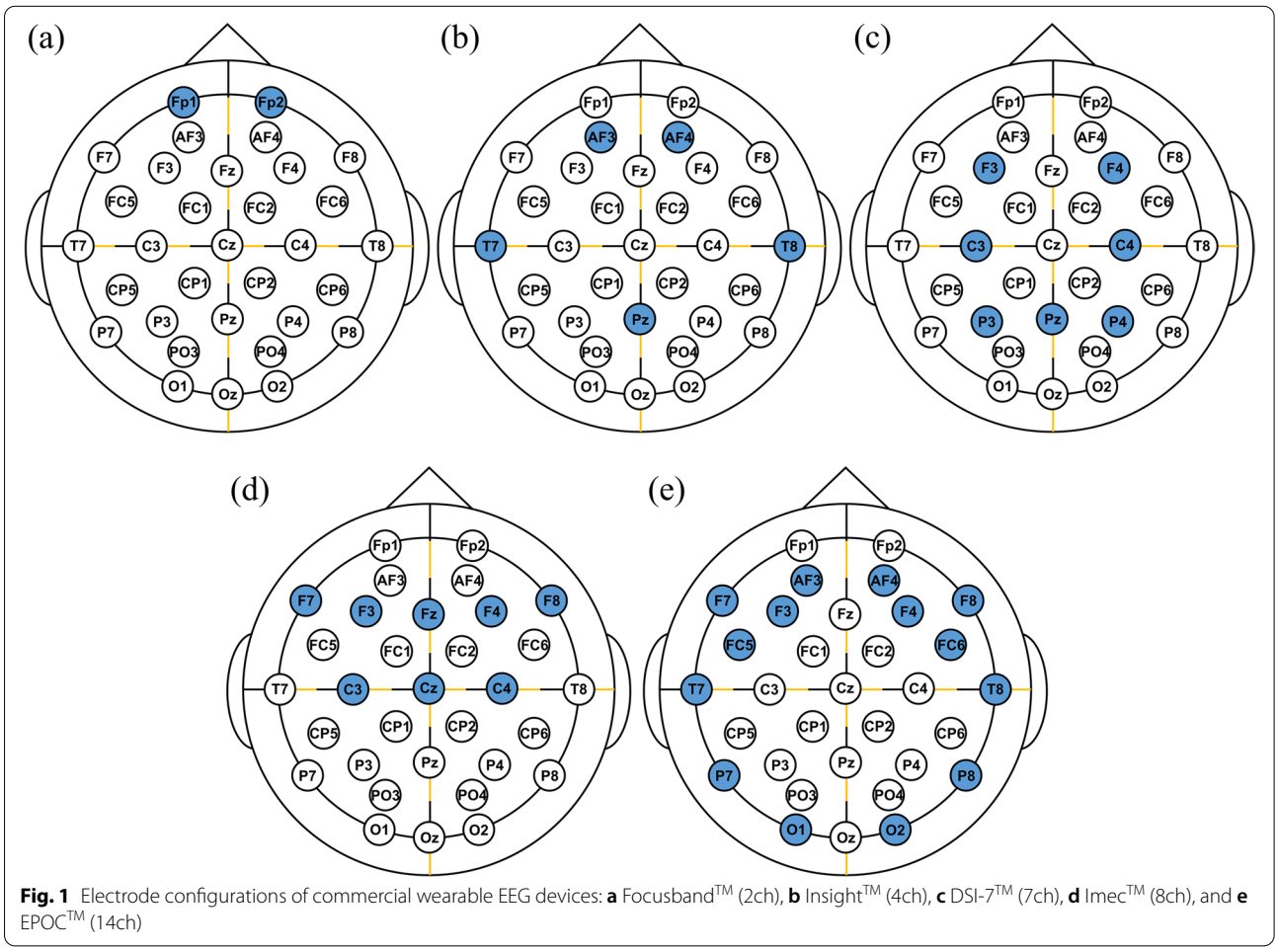

Fig. 1 Electrode configurations of commercial wearable EEG devices: **a** Focusband™ (2ch), **b** Insight™ (4ch), **c** DSI-7™ (7ch), **d** Imec™ (8ch), and **e** EPOC™ (14ch)

Table 1 Demographic information of the MCI and HC groups

	MCI	HC
N	21	21
Male / Female	7/14	6/15
p	0.7385	
Age		
Mean	74.71	73.71
(SD)	(6.50)	(4.63)
p	0.5686	
Education		
Mean	7.86	9.33
(SD)	(4.42)	(5.47)
p	0.3476	

is presented in Table 1. All participants signed a written informed consent form approved by the Inje University Ilsan Paik Hospital Institutional Review Board (IRB no. 2018-12-012-013).

Signal acquisition and preprocessing

The EEG signal was acquired at a rate of 1000 Hz using a SynAmps amplifier (Neuroscan, Compumedics USA, Charlotte, NC, USA) from 32 scalp electrodes (Fp1, Fp2, AF3, AF4, Fz, F3, F4, F7, F8, FC1, FC2, FC5, FC6, Cz, C3, C4, T7, T8, CP1, CP2, CP5, CP6, Pz, P3, P4, P7, P8, PO3, PO4, Oz, O1, and O2) according to the modified international 10–20 system. The impedance of each electrode was maintained below 5 kΩ throughout the experimental period. Ground and reference electrodes were placed on the forehead and mastoids.

The resting EEG was recorded for 4 min with eyes closed. The acquired EEG data were manually inspected to eliminate blocks contaminated by environmental or physiological noise. Then the EEG data were baseline-corrected by subtracting the average value for each channel and band-pass filtered at cut-off frequencies of 0.5 Hz and 50 Hz using a 6th-order zero-phase Butterworth infinite impulse response filter. Thereafter, the preprocessed resting EEG data were segmented into 5-s epochs without an overlap. We rejected epochs in which the maximal absolute potential value exceeded the threshold of 75 μV; therefore, the numbers of remaining epochs were different among subjects, with twenty being the minimal number of epochs. To equalize the number of epochs for each subject, twenty epochs were randomly selected for each subject.

Feature extraction

The absolute power spectrum density (APSD), relative power spectrum density (RPSD), differential asymmetry (DASM), rational asymmetry (RASM), phase-amplitude coupling (PAC), Shannon entropy (SE), Hjorth parameters (HP), Lyapunov exponent (LE), Hurst exponent (HE), and Kolmogorov complexity (KC) were extracted as candidate features for MCI diagnosis. These candidate features have been used as biomarkers in previous studies on EEG-based diagnosis of MCI or Alzheimer's disease (AD) [17, 34–37]. The equations used to compute these features are summarized in Table 2, and their derivation process and detailed description are provided in the Supplementary Material.

Spectral features were calculated for each of the following nine sub-frequency bands: delta (δ, 1–4 Hz), theta (θ, 4–8 Hz), low alpha (α_L, 8–10 Hz), high alpha (α_H, 10–12 Hz), total alpha (α, 8–12 Hz), low beta (β_L, 12–18 Hz), high beta (β_H, 18–30 Hz), total beta (β, 12–30 Hz), and gamma (β, 30–50 Hz).

For the PAC, which evaluates the coherence between the low-frequency phase and high-frequency amplitude, the low-frequency signal was set as either δ or θ, while the high-frequency signal was set as one of the other seven sub-frequency bands (except δ or θ). The total number of candidate features extracted from the 32 channels was 1500 consisting of {9 (APSD) + 9 (RPSD) + 14 (PAC) + 3 (HP) + 1 (SE) + 1 (LE) + 1 (HE) + 1(KC)} × 32(channels) + {9 (DASM) + 9 (RASM)} × 14 (pairs). Each candidate feature was averaged over all twenty epochs per channel, resulting in 1500 averaged candidate features per participant.

Feature selection and classification

A support vector machine (SVM) classifier was employed using the statistics and machine learning toolbox in MATLAB 2018b (MathWorks, Natick, MA, USA). Leave-pair-out (LPO) cross-validation (CV) was conducted to evaluate the classification accuracy of the model [44]. In detail, the data of two participants (one patient with MCI and one from the HC group) were used as the test set, and the data of the remaining 40 participants (20 patients with MCI and 20 HCs) were used as the training set. Accuracy, sensitivity, and specificity were calculated and averaged over all possible combinations of the two participants (one MCI and one HC; $21 \times 21 = 441$).

In each iteration of LPO-CV, z-score normalization was applied to each feature of the training set [45]:

$$z = \frac{X - \overline{X}}{\sigma}, \tag{1}$$

where $\overline{X}$ and σ denote mean and standard deviation, respectively. The features of the test set were normalized using (1) with the $\overline{X}$ and σ calculated from the training set. The optimal feature subset was then selected from the training set based on the rank order according to

Table 2 List of EEG features evaluated in this study

Feature	Mathematical expression
Absolute power spectrum density (APSD)[a]	$\frac{1}{N}\sum_{n=1}^{N} x(n)e^{-i2\pi fn/N}$
Relative power spectrum density (RPSD)	Absolute PSD of specific band/absolute PSD of total band
Differential asymmetry (DASM) [32]	Difference between absolute PSDs of inter-hemispheric electrode pairs
Rational asymmetry (RASM) [32]	Ratio between absolute PSDs of inter-hemispheric electrode pairs
Phase-amplitude coupling (PAC)[b] [38]	$\text{coherence}_{fph}\left(X_{ph}, \widetilde{A}_{ph}\right)$
Shannon entropy (SE) [39]	$-\sum_{i=1}^{N} p(x_i)\ln p(x_i)$, where $\sum_{i=1}^{N} \text{p}(\text{x}_\text{i}) = 1$
Hjorth parameters (HP)[c] [40]	$\textbf{Activity}(\boldsymbol{x}) = \frac{1}{N}\sum_{i=1}^{N}(x_i-\mu_i)^2$ $\textbf{Mobility}(\boldsymbol{x}) = \sqrt{\frac{\sigma(x')}{\sigma(x)}}$ $\textbf{Complexity}(\boldsymbol{x}) = \frac{\text{Mobility}(x')}{\text{Mobility}(x)}$
Lyapunov exponent (LE)[d] [41]	$\lambda(i) = \frac{1}{i\Delta t}\frac{1}{K}\sum_{j=1}^{K}\ln\frac{d_j(i)}{d_j(0)}$
Hurst exponent (HE)[e] [42]	$\log(R/S)/\log(N)$
Kolmogorov complexity[f] **(KC)** [43]	$c(n)/b(n)$

x represents the EEG time-series data and [a]*N* indicates the length of the data. [b] The coherence here is the coherence at frequency *fph* between the time-varying energy of the high-frequency signal (A_{ph}) and the unfiltered raw signal believed to contain the modulating frequency (X_{ph}), [c]μ_i represents the mean of *x*, *x*′ represents the derivative of *x*, and $\sigma(x)$ represents the standard deviation of *x*. [d] Δt is the sampling period of the EEG time series, *K* is the embedding dimension, $d_j(0)$ is the initial distance from the *j*th point to its nearest neighbor, and $d_j(i)$ is the distance between the *j*th pair of nearest neighbors after *i* discrete time steps. [e]*N* is the length of the data sample, *R* is the difference between the maximum deviation from the mean and the minimum deviation from the mean, and *S* is the standard deviation. [f]*n* is the length of the time-series data, $c(n)$ reflects the relative complexity of the data, and $b(n)$ is the ratio between n and $\log(n)$. The details are described in the Supplementary Material

Fisher's score, which is one of the most widely used filter methods for supervised feature selection [46]. The feature selection was performed with the candidate features extracted from the target electrode configuration. The maximum number of selected features was set to 15 to avoid potential overfitting. The "*N*-feature accuracy" was evaluated by averaging the results of all LPO-CV iterations for *N* features, where *N* represents the number of features used for the classification, which ranged from 1 to 15. The classification accuracy for each electrode configuration was determined as the highest accuracy among the "*N*-feature accuracies." Note that the highest accuracy was achieved when the number of features was less than 10 in most cases.

Statistical analysis

Statistical analysis was conducted to investigate the differences in demographic information between the MCI and HC groups and differences in the classification accuracies between the proposed optimal electrode configurations and those of commercial wearable EEG devices. The chi-square test [47] was conducted to test the difference in sex composition between the MCI and HC groups. A two-tailed Student's *t*-test [48] was conducted to identify the differences in age and education between the MCI and HC groups as the normality of the data was confirmed by the one-sample Kolmogorov–Smirnov test [49]. In addition, the Bonferroni-corrected Wilcoxon signed-rank test [50, 51] was conducted to identify the difference between the classification accuracies for the proposed electrode configurations and those of the commercial wearable EEG devices as the normality of the data was not confirmed by the one-sample Kolmogorov–Smirnov test.

Results

The optimal electrode configurations that resulted in the highest classification accuracy among all possible channel combinations are presented in Table 3 and Fig. 2a. The optimal two-channel (hereafter denoted by Opt-2ch), four-channel (Opt-4ch), six-channel (Opt-6ch), and eight-channel (Opt-8ch) electrode configurations were "F3–F4," "AF3–AF4–FC5–FC6," "FC5–FC6–C3–C4–P7–P8," and "F3–F4–FC5–FC6–C3–C4–P7–P8," respectively. All optimal electrode configurations were composed of combinations of the following five electrode pairs: AF3–AF4, F3–F4, FC5–FC6, C3–C4, and P7–P8, which were in the frontal and parietal areas. Notably, Opt-8ch was a combination of Opt-2ch and Opt-6ch, and no midline electrode was included in the optimal electrode configuration.

Table 3 Channel combination and diagnostic performances of the optimal electrode configurations and those of five commercial wearable EEG devices

	Accuracy (Mean±SD)	Sensitivity (Mean±SD)	Specificity (Mean±SD)	Channel combination
Opt-2ch	74.04% ±4.82	63.95% ±9.23	84.13% ±7.87	F3–F4
Opt-4ch	82.43% ±6.14	70.75% ±11.98	94.10% ±4.23	AF3–AF4–FC5–FC6
Opt-6ch	86.28% ±2.81	86.17% ±6.55	86.39% ±5.28	FC5–FC6–C3–C4–P7–P8
Opt-8ch	86.85% ±4.97	86.85% ±6.88	86.85% ±7.81	F3–F4–FC5–FC6–C3–C4–P7–P8
Focusband™(2ch)	55.90% ±7.01	50.11% ±12.01	61.68% ±8.71	Fp1–Fp2
Insight™(5ch)	61.22% ±7.97	55.10% ±13.58	67.35% ±9.07	Pz–AF3–AF4–T7–T8
DSI-7™(7ch)	64.74% ±7.17	65.76% ±11.72	63.72% ±8.84	Pz–F3–F4–C3–C4–P3–P4
Imec™(8ch)	74.15% ±6.87	70.29% ±10.85	78.00% ±9.58	Fz–Cz–F7–F8–F3–F4–C3–C4
Epoc™(14ch)	73.81% ±7.57	60.77% ±12.41	86.85% ±7.21	AF3–AF4–F7–F8–F3–F4–FC5–FC6–T7–T8–P7–P8–O1–O2

LPO-CV can be regarded as the 21 × 21-fold cross-validation. Therefore, the results of 441 iterations of LPO-CV were first divided into 21 blocks, and then the standard deviation (SD) was calculated across the 21 blocks

The accuracy, sensitivity, and specificity of the machine learning-based MCI diagnosis using optimal electrode configurations are summarized in Table 3. The numbers of features that resulted in the highest accuracies were 2, 2, 6, and 7 for Opt-2ch, Opt-4ch, Opt-6ch, and Opt-8ch, respectively. Accuracies of 74.04% ± 4.82, 82.43% ± 6.14, 86.28% ± 2.81, and 86.85% ± 4.97 were achieved for Opt-2ch, Opt-4ch, Opt-6ch, and Opt-8ch, respectively, which demonstrated the possibility of precise machine learning-based diagnosis of MCI with a limited number of EEG electrodes. It can be seen from the table that the classification accuracy gradually increases as the number of electrodes increases; however, the increment in the accuracy is nearly saturated when the number of electrodes becomes six. Furthermore, while the sensitivity was approximately 20% lower than the specificity for Opt-2ch and Opt-4ch, the difference between the sensitivity and specificity was reduced to less than 1% for Opt-6ch and Opt-8ch.

The accuracy, sensitivity, and specificity of the machine learning-based MCI diagnosis using the electrode configurations of the five commercial wearable EEG devices are provided in Table 3. A statistical comparison of the classification accuracies between the four optimal electrode configurations and the five wearable EEG devices is shown in Fig. 2b. Opt-2ch statistically outperformed the electrode configurations of three commercial devices (Focusband™, Insight™, and DSI-7™, Bonferroni-corrected $p < 0.001$) that were composed of two, five, and seven electrodes, respectively. Opt-2ch did not show significant improvement compared to Imec™ (Bonferroni-corrected $p = 0.94$) and EPOC™ (Bonferroni-corrected $p = 0.88$), which are composed of eight and 14 electrodes, respectively. The other optimal electrode configurations (Opt-4ch, Opt-6ch, and Opt-8ch) statistically outperformed the electrode configurations of all the commercial wearable EEG devices considered in this study (Bonferroni-corrected $p < 0.001$ in all cases).

Figure 3 shows the 3D-rendered concept design of wearable EEG devices with the proposed optimal electrode configuration. 3D images were rendered using Maya 2022 (Autodesk Inc., San Rafael, CA, USA). The overall design concept was inspired by EPOC™ (Emotiv Inc.; San Francisco, CA, USA). In addition, the devices were assumed to have fingered EEG electrodes, which reflected the latest trend in electrode design for wearable EEG devices [24].

Discussion

In this study, we attempted to determine the optimal electrode configurations that could lead to the highest accuracy in the machine-learning-based diagnosis of MCI. The electrode configurations investigated in this study were composed of a small number of electrodes (two, four, six, and eight electrodes), assuming wearable EEG devices can potentially be utilized for daily life monitoring of MCI. The proposed optimal electrode configurations showed statistically higher accuracies

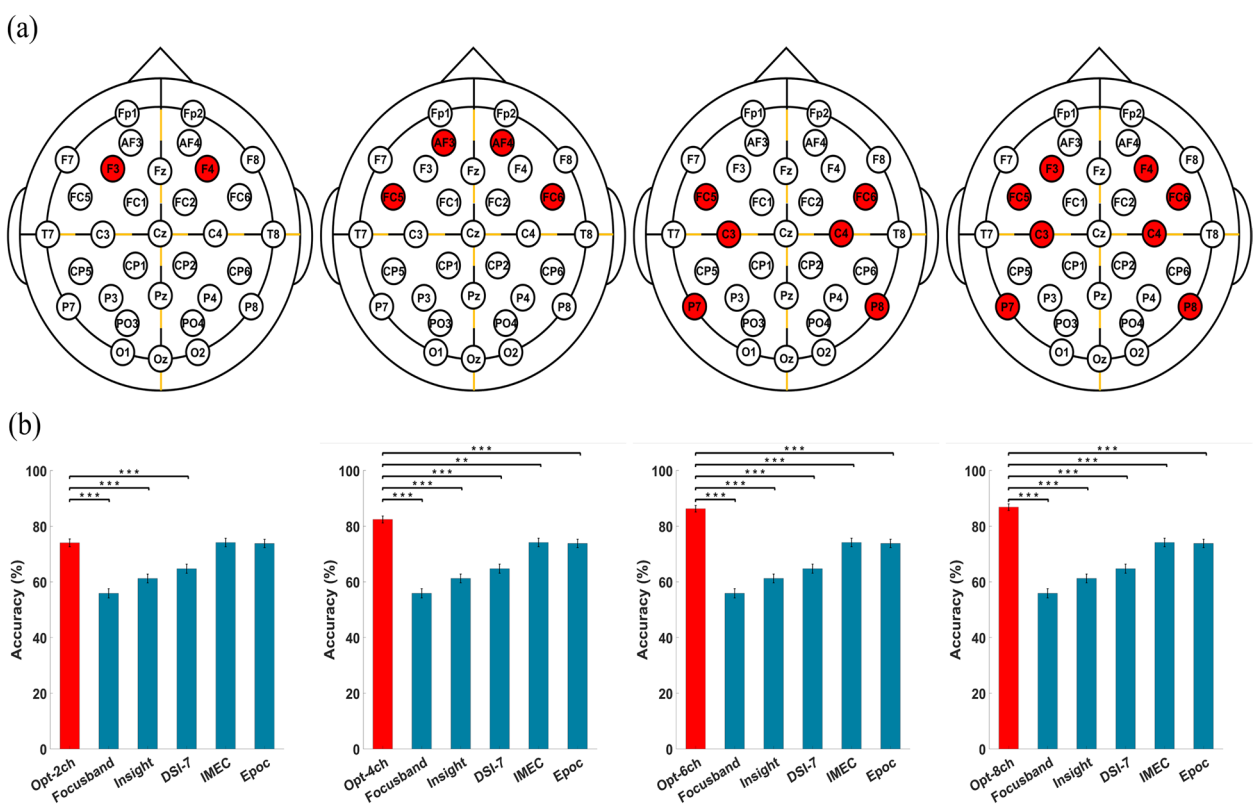

Fig. 2 **a** Proposed optimal electrode configurations consisting of two, four, six, and eight channels (from top to bottom). **b** Performance comparison between the proposed optimal electrode configurations and the electrode configurations of commercial wearable EEG devices. The *x*-axis of the bar graphs represents the electrode configurations. The error bars indicate standard error. * Bonferroni-corrected $p < 0.05$, ** Bonferroni-corrected $p < 0.001$, *** Bonferroni-corrected $p < 0.0001$

than the electrode configurations of commercial wearable EEG devices, albeit with a smaller number of electrodes. For example, Opt-4ch showed a higher diagnostic accuracy than the electrode configurations of all five commercial wearable EEG devices tested in this study, which highlighted the importance of optimizing the electrode configurations in the design of wearable EEG devices considering the specific purpose of the wearable EEG devices.

We investigated the most frequently selected features in the LPO-CV iterations to identify the EEG features that contributed the most to distinguishing between patients with MCI and HCs. Table 4 shows the four most frequently selected features and their mean values for the MCI and HC groups. The four features were δ DASM between FC5 and FC6, the HE in F3, the HE in C4, and PAC (θ-β_H) in P8, which were selected at least 397 times out of 441 LPO-CV iterations (approximately 90% of all LPO-CV iterations) for Opt-8ch (see Supplementary Fig. 1). These EEG features have been found to be closely associated with the pathophysiology of MCI in previous studies.

First, the value of δDASM between FC5 and FC6 in patients with MCI was statistically higher than that in the HCs. This result is in line with a previous study that reported that patients with MCI exhibited a significantly higher delta-band power in the left central area than HCs; however, this was not the case for the right central area [52]. Additionally, the HE in F3 and C4 was significantly higher in the MCI group than in the HC group in our study. These results are also in good agreement with those of previous studies. According to John et al. [53], the HE of patients with MCI or AD was higher than that of the HCs in whole-brain areas when the HE values were calculated from eyes-closed resting EEG data, as in our study. Lastly, the PAC (θ-β_H) at P8 was lower in patients with MCI than in the HCs in our study. This result is also consistent with that of Poza et al. [54] reported that patients with mild AD exhibited lower PAC values in the posterior area than HCs.

Although the proposed optimal electrode configurations exhibited statistically higher performance than the electrode configurations of commercial wearable EEG devices, their sensitivities were reported to be

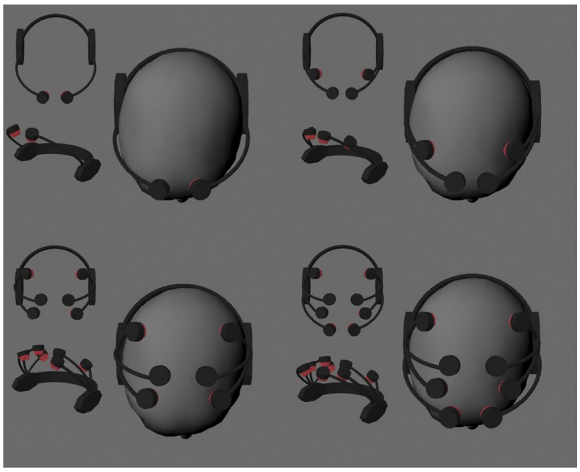

Fig. 3 3D-rendered images of wearable EEG devices with the electrode configurations proposed in this study

approximately 20% lower than the specificities in cases of Opt-2ch and Opt-4ch. In general, well-balanced sensitivity and specificity values are important in designing diagnostic systems. However, as wearable EEG devices are expected to be employed as tools for the primary screening of MCI, an EEG device with higher diagnostic sensitivity is required. Therefore, these optimal electrode configurations could be alternatively determined by selecting the electrode combinations with the highest sensitivity with the overall accuracy maintained at an appropriate level. For example, an electrode pair "C3–C4" showed a classification accuracy of 69.16% ± 7.55, which is approximately 5%p lower than that of Opt-2ch; however, it showed a relatively higher sensitivity of 74.60% ± 11.30 and a moderate level of specificity (63.72% ± 9.58) (see Supplementary Table 1). In the case of the 4-channel configuration, "F3–F4–FC5–FC6" showed an approximately 8% higher sensitivity than Opt-4ch when the difference in accuracy between the two configurations was only 2.5%p (see Supplementary Table 2). If sensitivity is regarded as a more important factor than specificity in designing wearable EEG devices for the primary screening of MCI, the "C3–C4" and "F3–F4–FC5–FC6" configurations might be considered possible alternatives to Opt-2ch and Opt-4ch, respectively. The top 20 electrode configurations for six- and eight-electrode cases can also be found in Supplementary Tables 3 and 4.

The optimal electrode configurations for the diagnosis of MCI may vary depending on several factors, such as the participants and recording devices. Because most EEG features have large inter-subject and/or

Table 4 Comparisons of the most frequently selected feature values between the MCI and HC groups

Feature list	MCI (mean ± SD)	HC (mean ± SD)	*p*-value
DASM (δ) between FC5 and FC6 (μV^2)	0.4687 ± 0.4653	0.0953 ± 0.1045	** 0.0016
HE in F3	0.7806 ± 0.0664	0.7288 ± 0.0505	** 0.0063
PAC (θ-β_H) in P8	0.1172 ± 0.0100	0.1281 ± 0.0141	* 0.025
HE in C4	0.7464 ± 0.0624	0.6948 ± 0.0582	** 0.0054

Statistical analysis was performed using a two-tailed Student's *t*-test, as the normality of each compared feature was confirmed using the one-sample Kolmogorov–Smirnov test. * $p < 0.05$, ** $p < 0.01$, *** $p < 0.001$

inter-device variability [55], an additional EEG dataset acquired from a larger number of participants using various EEG devices might be necessary in future studies to further generalize the proposed electrode configurations. It is expected that the optimal electrode configurations will be fine-tuned based on an additional EEG dataset. Additionally, we are planning to manufacture a wearable EEG device with the proposed optimal electrode configuration and investigate in a future study whether the device is effective enough to be used for the early screening of MCI.

Supplementary Information

The online version contains supplementary material available at https://doi.org/10.1186/s13195-022-01115-3.

Additional file 1: Supplementary Table 1. Performances of the top 10 electrode configurations composed of two electrodes. The table lists the calculated accuracies, sensitivities, and specificities for the top 10 electrode configurations with the highest accuracies. These values were used as performance measures. **Supplementary Table 2.** Performances of the top 10 electrode configurations composed of four electrodes. The table lists the calculated accuracies, sensitivities, and specificities for the top 10 electrode configurations with the highest accuracies. These values were used as performance measures. **Supplementary Table 3.** Performances of the top 20 electrode configurations composed of six electrodes. The table lists the calculated accuracies, sensitivities, and specificities for the top 20 electrode configurations with the highest accuracies. These values were used as performance measures. **Supplementary Table 4.** Performances of the top 20 electrode configurations composed of eight electrodes. The table lists the calculated accuracies, sensitivities, and specificities for the top 20 electrode configurations with the highest accuracies. These values were used as performance measures. **Supplementary Figure 1.** List of the most frequently selected features. The features were most frequently selected in all CV iterations for the number of features that yielded the highest accuracy in each optimal electrode configuration. From top to bottom, the feature list of the Opt-2ch, Opt-4ch, Opt6ch, and Opt-8ch configurations are described. The x-axis is "oftenness," which is calculated by dividing the feature selection times by all CV iteration times (441).

Authors' contributions
C. H. Im conceived the study concept and designed the study. S. H. Lee provided the data. K. G. Lee constructed the machine learning designs, conducted statistical analyses, and drafted the manuscript. K.G. Lee and K.M. Choi contributed to the preprocessing of data. S. H. Park and K. G. Lee extracted the

features from the data. All the authors have revised the manuscript accordingly. The author(s) read and approved the final manuscript.

Funding
This work was supported in part by a National Research Foundation of Korea (NRF) grant funded by the Korean government (MSIT) (No. NRF-2019R1A2C2086593) and a Korea Medical Device Development Fund grant funded by the Korean government (No. 202013B10).

Availability of data and materials
The data used in this study cannot be open to the public according to the Institutional Review Board approval.

Declarations

Ethics approval and consent to participate
The study protocol was approved by the Inje University Ilsan Paik Hospital Institutional Review Board (IRB no. 2018-12-012-013) and the study was conducted in accordance with the Declaration of Helsinki. All participants signed a written informed consent form before their participation in the study.

Consent for publication
Not applicable

Competing interests
The authors declare that they have no competing interests.

Author details
[1]School of Electronic Engineering, Hanyang University, Seoul, Republic of Korea. [2]Department of Psychiatry, Inje University Ilsan Paik Hospital, Goyang, Republic of Korea. [3]Clinical Emotion and Cognition Research Laboratory, Inje University Ilsan Paik Hospital, Goyang, Republic of Korea. [4]School of Biomedical Engineering, Hanyang University, Seoul, Republic of Korea.

Received: 23 August 2022 Accepted: 31 October 2022
Published online: 12 November 2022

References

1. Gauthier S, et al. Mild cognitive impairment. Lancet. 2006;367(9518):1262–70.
2. Ieracitano C, et al. A novel multi-modal machine learning based approach for automatic classification of EEG recordings in dementia. Neural Netw. 2020;123:176–90.
3. World Health Organization. Meeting on the Implementation of the global action plan of the public health response on dementia 2017-2025: meeting report: 11-12 December 2017. Geneva: World Health Organization; 2018.
4. Luck T, et al. Incidence of mild cognitive impairment: a systematic review. Dementia Geriatr Cognitive Disord. 2010;29(2):164–75.
5. Chen W, Wang H. Mild cognitive impairment: a concept useful for early detection and intervention of dementia. Shanghai Arch Psychiatry. 2013;25(2):119.
6. Pedrosa H, et al. Functional evaluation distinguishes MCI patients from healthy elderly people—the ADCS/MCI/ADL scale. J Nutr Health Aging. 2010;14(8):703–9.
7. Sabbagh MN, et al. Early detection of mild cognitive impairment (MCI) in primary care. J Prev Alzheimer's Dis. 2020;7(3):165–70.
8. Edmonds EC, et al. "Missed" mild cognitive impairment: High false-negative error rate based on conventional diagnostic criteria. J Alzheimer's Dis. 2016;52(2):685–91.
9. Roberts R, Knopman DS. Classification and epidemiology of MCI. Clin Geriatr Med. 2013;29(4):753–72.
10. Stomrud E, et al. Slowing of EEG correlates with CSF biomarkers and reduced cognitive speed in elderly with normal cognition over 4 years. Neurobiol Aging. 2010;31(2):215–23.
11. Vemuri P, et al. MRI and CSF biomarkers in normal, MCI, and AD subjects: predicting future clinical change. Neurology. 2009;73(4):294–301.
12. Stam C, et al. EEG synchronization in mild cognitive impairment and Alzheimer's disease. Acta Neurol Scand. 2003;108(2):90–6.
13. König T, et al. Decreased EEG synchronization in Alzheimer's disease and mild cognitive impairment. Neurobiol Aging. 2005;26(2):165–71.
14. Baker M, et al. EEG patterns in mild cognitive impairment (MCI) patients. Open Neuroimaging J. 2008;2:52.
15. Sharma N, et al. EEG and cognitive biomarkers based mild cognitive impairment diagnosis. IRBM. 2019;40(2):113–21.
16. Poil S-S, et al. Integrative EEG biomarkers predict progression to Alzheimer's disease at the MCI stage. Front Aging Neurosci. 2013;5:58.
17. Cassani, Raymundo, et al. Systematic review on resting-state EEG for Alzheimer's disease diagnosis and progression assessment. Dis Markers. 2018;2018:5174815.
18. Trambaiolli LR, et al. Improving Alzheimer's disease diagnosis with machine learning techniques. Clin EEG Neurosci. 2011;42(3):160–5.
19. Kashefpoor M, Rabbani H, Barekatain M. Automatic diagnosis of mild cognitive impairment using electroencephalogram spectral features. J Med Sign Sensors. 2016;6(1):25.
20. Morabito, Francesco Carlo, et al. Deep convolutional neural networks for classification of mild cognitive impaired and Alzheimer's disease patients from scalp EEG recordings. In: 2016 IEEE 2nd International Forum on Research and Technologies for Society and Industry Leveraging a better tomorrow (RTSI). IEEE; 2016. p. 1-6.
21. Fiscon G, et al. Combining EEG signal processing with supervised methods for Alzheimer's patients classification. BMC Med Inform Decis Making. 2018;18(1):1–10.
22. Casson AJ, et al. Wearable electroencephalography. IEEE Eng Med Biol Magazine. 2010;29(3):44–56.
23. Duvinage M, et al. A P300-based quantitative comparison between the Emotiv Epoc headset and a medical EEG device. Biomed Eng. 2012;765(1):2012–764.
24. Casson AJ. Wearable EEG and beyond. Biomed Eng letters. 2019;9(1):53–71.
25. Debener S, et al. How about taking a low-cost, small, and wireless EEG for a walk? Psychophysiology. 2012;49(11):1617–21.
26. Mihajlović V, et al. Wearable, wireless EEG solutions in daily life applications: what are we missing? IEEE J Biomed Health Inform. 2014;19(1):6–21.
27. Gaidar V, Sudakov O. Design of wearable EEG device for seizures early detection. Int J Electron Telecommun. 2021;67(2):187–92.
28. Samuel N, et al. Consumer-grade electroencephalography devices as potential tools for early detection of brain tumors. BMC Medicine. 2021;19(1):1–3.
29. Hsieh, Ju-Chun, et al. Design of hydrogel-based wearable EEG electrodes for medical applications. J Materials Chem B. 2022;10:7260–80.
30. Ingolfsson, Thorir Mar, et al. Towards long-term non-invasive monitoring for epilepsy via wearable eeg devices. In: 2021 IEEE Biomedical Circuits and Systems Conference (BioCAS). IEEE; 2021. p. 01–04.
31. Arvaneh, Mahnaz, et al. Robust EEG channel selection across sessions in brain-computer interface involving stroke patients. In: The 2012 International Joint Conference on Neural Networks (IJCNN). IEEE; 2012. p. 1–6.
32. Park S, Han C-H, Im C-H. Design of wearable EEG devices specialized for passive brain–computer interface applications. Sensors. 2020;20(16):4572.
33. Abdullah, Muhammad Kamil, et al. Analysis of effective channel placement for an EEG-based biometric system. In: 2010 IEEE EMBS Conference on Biomedical Engineering and Sciences (IECBES). IEEE; 2010. p. 303–306.
34. McBride JC, et al. Spectral and complexity analysis of scalp EEG characteristics for mild cognitive impairment and early Alzheimer's disease. Comp Methods Prog Biomed. 2014;114(2):153–63.
35. Dimitriadis SI, et al. A novel biomarker of amnestic MCI based on dynamic cross-frequency coupling patterns during cognitive brain responses. Front Neurosci. 2015;9:350.
36. Houmani N, Dreyfus G, Vialatte FB. Epoch-based entropy for early screening of Alzheimer's disease. Int J Neural Syst. 2015;25(08):1550032.
37. Garn H, et al. Differential diagnosis between patients with probable Alzheimer's disease, Parkinson's disease dementia, or dementia with Lewy bodies and frontotemporal dementia, behavioral variant, using quantitative electroencephalographic features. J Neural Trans. 2017;124(5):569–81.
38. Osipova D, Hermes D, Jensen O. Gamma power is phase-locked to posterior alpha activity. PloS One. 2008;3(12):e3990.
39. Shannon CE. A mathematical theory of communication. Bell Syst Tech J. 1948;27(3):379–423.
40. Hjorth B. The physical significance of time domain descriptors in EEG analysis. Electroencephalography Clin Neurophysiol. 1973;34(3):321–5.

41. Rosenstein MT, Collins JJ, De Luca CJ. A practical method for calculating largest Lyapunov exponents from small data sets. Physica D Nonlinear Phenomena. 1993;65(1-2):117–34.
42. Feder J. Fractals. New York: Plenum Press; 2013.
43. Kolmogorov AN. Three approaches to the definition of the concept "quantity of information". Probl Peredachi Informatsii. 1965;1(1):3–11.
44. Smith GC, et al. Correcting for optimistic prediction in small data sets. Am J Epidemiol. 2014;180(3):318–24.
45. Jain A, Nandakumar K, Ross A. Score normalization in multimodal biometric systems. Pattern Recogn. 2005;38(12):2270–85.
46. Gu Q, Li Z, Han J. Generalized fisher score for feature selection. arXiv preprint arXiv:1202.3725. 2012.
47. McHugh ML. The chi-square test of independence. Biochem Med. 2013;23(2):143–9.
48. Hsu H, Lachenbruch PA. Lachenbruch. Paired t test. Wiley StatsRef: statistics reference online. 2014.
49. Lilliefors HW. On the Kolmogorov-Smirnov test for normality with mean and variance unknown. J Am Stat Assoc. 1967;62(318):399–402.
50. Woolson RF. Wilcoxon signed-rank test. Wiley encyclopedia of clinical trials. 2007. p. 1–3.
51. Bland JM, Altman DG. Multiple significance tests: the Bonferroni method. Bmj. 1995;310(6973):170.
52. Kwak YT. Quantitative EEG findings in different stages of Alzheimer's disease. J Clin Neurophysiol. 2006;23(5):457–62.
53. John TN, Puthankattil SD, Menon R. Analysis of long range dependence in the EEG signals of Alzheimer patients. Cogn Neurodynam. 2018;12(2):183–99.
54. Poza J, et al. Phase-amplitude coupling analysis of spontaneous EEG activity in Alzheimer's disease. In: 2017 39th Annual International Conference of the IEEE Engineering in Medicine and Biology Society (EMBC). IEEE; 2017. p. 2259–2262.
55. Takeuchi I, et al. Transdermal delivery of estradiol-loaded PLGA nanoparticles using iontophoresis for treatment of osteoporosis. Bio Med Mater Eng. 2016;27(5):475–83.

Publisher's Note